# Isolating the atrial component from ECG and MCG recordings of periodic tachyarrhythmias

Eduardo Andrade Lima*, Dan Marchesin

Instituto Nacional de Matemática Pura e Aplicada
Estrada Dona Castorina 110, Rio de Janeiro, RJ 22460-320, Brazil
(e-mails: *eduardo.a.lima@vanderbilt.edu*, *marchesi@fluid.impa.br*)

## ABSTRACT

We present a technique to retrieve the component associated with atrial cardiac activity from electrocardiogram (ECG) and magnetocardiogram (MCG) recordings of periodic tachyarrhythmias. We use a suitable time window to remove the ventricular component and by a deconvolution we successfully recover the atrial activity over the whole recording, even for narrow windows or high noise levels. Two approaches for the deconvolution problem are investigated. The performance of these approaches is analyzed using synthetic recordings, either noiseless signals or signals corrupted by white noise. The technique is tested on atrial flutter ECG and MCG recordings.

## I. INTRODUCTION

The investigation of electrical propagation patterns in cardiac tissue can give invaluable information on the mechanisms governing many cardiac pathologies. In particular, the study of certain periodic atrial tachyarrhythmias is of importance as they can lead to sudden death when

* Present Address: Department of Biomedical Engineering - VIIBRE Institute, Vanderbilt University, 6301 Stevenson Center, Nashville, TN, 37235.

taking place at the ventricles [1]-[3]. Furthermore, understanding anomalous propagation in these arrhythmias might aid in developing new therapeutic procedures.

Invasive electrogram recordings are obtained by an array of electrodes placed in direct contact with the heart tissue to measure the electric potential. A non-invasive alternative is magnetocardiography [4]-[6], in which measurements of the magnetic field associated with the electrical propagation are performed by a high sensitivity superconducting magnetometer, known as SQUID sensor [7], at a grid of positions over the heart. The magnetic field recordings can then be used as input data for an algorithm for finding the distribution of the field sources, thus providing a picture of the electrical activity. Since the magnetic field at a fixed position varies with time, the inverse problem is usually difficult to solve and different methods have been tried. Because the SQUID sensor can be placed several centimeters away from the heart tissue and it does not interfere with the electrical activity propagation, magnetocardiography is a promising tool in the study of cardiac electrophysiology and in non-invasive clinical diagnosis.

For some relevant periodic tachyarrhythmias, the source of abnormal propagation lies in the atria and, thus, it is necessary to isolate the signal component related to atrial activity. The signal processing presented here can be used for both ECG and MCG recordings. Although our main motivation is the magnetocardiography inverse problem, there are many other situations in which the extraction of atrial component from MCG or ECG recordings can be of utility. Moreover, because the technique is fairly general, it can be used to isolate a periodic signal from the superposition of two signals, provided that the unwanted component can be eliminated through a time-periodic windowing operation.

Usually, conventional linear filtering is unsuitable for removing ventricular activity, such as QRST complexes, as the spectrums of desired and undesired signals often overlap. Hence, several alternative techniques have been proposed to address this issue.

Adaptive filtering was used to single-out atrial fibrillation signal in ECG recordings [8] but the cancellation scheme cannot fully remove the ventricular activity and some artifacts are left in lieu of the associated QRST complexes.

The Average Beat Subtraction approach (ABS) has been used to cancel the ventricular component in atrial fibrillation ECG recordings [9], [10]. The key idea is to calculate an average QRST complex and then to align and subtract instances of this median ventricular activity from all the QRST complexes present in the recording. Since atrial activity is unsynchronized with ventricular activity in atrial fibrillation, the remaining signal contains mostly fibrillation waveforms. Again, artifacts and distortions may be left where QRST complexes have been removed.

Recently, an improvement on the ABS technique called Spatiotemporal QRST Cancellation was proposed [11], [12]. The effects of respiratory activity are minimized, as the method incorporates a vectorcardiographic loop alignment technique and uses information of adjacent leads of 12-lead ECG recordings in the cancellation procedure. Instead of a single average QRST complex, several templates can be used for subtraction, thereby yielding a more accurate fibrillation signal.

Both adaptive filtering and ABS techniques do not yield satisfactory results for inverse problem applications due to occurrence of artifacts and distortion in the processed signal. Although we believe the Spatiotemporal QRST Cancellation technique could be adapted for magnetocardiography purposes, we propose a simple and robust technique to isolate the atrial activity for the specific case of arrhythmias with periodic atrial component and whose ventricular component can be removed by a periodic time-window, leaving no artifacts. We demonstrate its capabilities on atrial flutter, a typical arrhythmia that exhibits such characteristics.

## II. THE DECONVOLUTION PROBLEM

Let $z$ be the sum of two periodic functions $u$ and $v$ of time, with common period $T_v$. Let us assume that their fundamental periods are $T_u$ and $T_v$, respectively, where $T_v = KT_u$ and $K$ is a positive integer. In our problem, the function $v$ with longer period is considered to be an undesired component that masks $u$ (see the first three plots in Fig. 1, for an example). Assume that almost all the power of $v$ is concentrated within the intervals $mT_v + T_a \le t - t_0 \le mT_v + T_b$, where $m \in \mathbb{Z}$ and $0 \le T_a < T_b \le T_v$ ; $0 \le t_0 < T_v$. In this paper we present a method for retrieving $u$ given $z$, $T_u$ and $T_v$. In practice, we assume that both fundamental periods can be estimated from $z$ either by inspection or by spectral analysis techniques.

Initially, we define a characteristic function $\chi$, or window, which is zero inside the intervals $mT_v + T_a \le t - t_0 \le mT_v + T_b$, $m \in \mathbb{Z}$, and equal to one outside, as depicted in the last plot of Fig. 1. (Note that $\chi$ is a function of $t$ that depends on $t_0$, $T_a$ and $T_b$.) Multiplying $z$ by $\chi$ we get a windowed function $w$ where nearly all $v$ has been wiped out:

$$w(t) = z(t)\chi(t) = u(t)\chi(t) + v(t)\chi(t) \cong u(t)\chi(t) . \tag{1}$$

Related to $\chi$ we also define a quantity that measures the number of periods of the original signal with shorter period $u$ preserved by the windowing process. The windowing ratio $\rho$ is defined as the ratio of the time interval the function $\chi$ is equal to one, within one period of $\chi$, and the period of $u$. That is, $\rho = \left[T_v - \left(T_b - T_a\right)\right] / T_u$ . If $\rho = K$, then $\chi$ is the constant unit function and there is no windowing at all. At the other extreme, for $\rho = 0$ the function $u$ is completely wiped out as $w \equiv 0$ .

When analyzing certain mathematical properties of the technique we may allow $\rho$ to reach the upper limit $K$, although this is physically meaningless, as it would imply either no

ventricular activity at all or gross cancellation errors. Thus, whenever $\rho$ is made large we assume that *v* is sufficiently concentrated in time so that nearly all its energy is wiped out by the windowing process.

Expanding *w*, *u* and $\chi$ in Fourier series with fundamental period $T_v$ we get (see Appendix)

$$w(t) = \sum_{n=-\infty}^{+\infty} \hat{w}_n e^{i\omega_0 nt} \quad ; \quad u(t) = \sum_{n=-\infty}^{+\infty} \hat{u}_n e^{i\omega_0 nt} \quad ; \quad \chi(t) = \sum_{n=-\infty}^{+\infty} \hat{\chi}_n e^{i\omega_0 nt} , \tag{2}$$

where $\{\hat{w}_n\}$, $\{\hat{u}_n\}$ and $\{\hat{\chi}_n\}$ are the Fourier coefficients for *w*, *u*, and $\chi$, respectively, and $\omega_0 = 2\pi/T_v$. Note that $\hat{u}_n = 0$ whenever *n* is not a multiple of *K*, since the actual fundamental period of *u* is $T_u = T_v/K$. Thus,

$$u(t) = \sum_{n=-\infty}^{+\infty} \hat{u}_{nK} e^{i\omega_0 nKt} . \tag{3}$$

Since $w(t) = u(t)\chi(t)$, the convolution relationship below holds

$$\text{for all } n: \sum_{j=-\infty}^{+\infty} \hat{\chi}_{n-j} \hat{u}_j = \sum_{j=-\infty}^{+\infty} \hat{\chi}_{n-jK} \hat{u}_{jK} = \hat{w}_n . \tag{4}$$

We see that the problem of finding *u* given *w*, i.e. inverting (4), is a deconvolution operation.

We consider two different methods to invert (4), which rely upon solving a system of linear equations whose size is determined by the estimated number of relevant elements of $\{\hat{u}_n\}$. The first method, or "decomposition" approach, consists of expressing (4) directly as a system of linear equations. In the second method, or "orthogonal projection" approach, we take $\{\hat{\chi}_n\}$ and its shifted versions as elements of a vector basis onto which $\{\hat{w}_n\}$ is projected in order to construct the associated system.

For simplicity, the ventricular component *v*(*t*) was assumed to be periodic in the previous development. However, we stress that this is not at all a requirement. Provided the ventricular

activity can be wiped out by a time-window $\chi$ of period $T_v$, (i.e. $v(t)\chi(t) \cong 0$ for all $t$), the technique works the same. The key point in the previous development is the assumption that $v(t)$ can be completely removed by a periodic window, which is clearly a much weaker condition than assuming that $v(t)$ itself is periodic.

### *A. THE DECOMPOSITION APPROACH*

Assuming that the first $M$ harmonics of $u$ are relevant, we have that $\sum_{j=-M}^{+M} \hat{\chi}_{n-jK}\hat{u}_{jK} \cong \hat{w}_n$: for each $n$ there corresponds a linear equation with unknowns $\hat{u}_{jK}$. Thus, we choose a set of $2M+1$ integer values for $n$ that provides independent linear equations over a wide range of values for $\rho$ and, therefore, a non-singular square matrix to be inverted.

The expression for the magnitude of the Fourier coefficients $\{\hat{\chi}_n\}$ is:

$$|\hat{\chi}_n| = \left|\frac{1}{n\pi}\sin\left(\frac{n\pi\rho}{K}\right)\right| = \frac{\rho}{K}\left|\operatorname{sinc}\left(\frac{n\rho}{K}\right)\right|, \tag{5}$$

where $n \in \mathbb{Z}$. We see that $|\hat{\chi}_n|$ decays as $n$ grows and $\hat{\chi}_0 = \rho/K$ is the coefficient with maximum magnitude. By choosing $n$ to span the set $\{-MK, (-M+1)K, \cdots, +MK\}$ the system of linear equations $\boldsymbol{Aq} = \boldsymbol{b}$ involves a Hermitian Toeplitz matrix:

$$\begin{bmatrix} \hat{\chi}_0 & \hat{\chi}_K & \cdots & \hat{\chi}_{2MK} \\ \overline{\hat{\chi}_K} & \hat{\chi}_0 & \cdots & \hat{\chi}_{(2M-1)K} \\ \vdots & \vdots & \cdots & \vdots \\ \overline{\hat{\chi}_{2MK}} & \overline{\hat{\chi}_{(2M-1)K}} & \cdots & \hat{\chi}_0 \end{bmatrix} \begin{bmatrix} \hat{u}_{-MK} \\ \hat{u}_{(-M+1)K} \\ \vdots \\ \hat{u}_{MK} \end{bmatrix} = \begin{bmatrix} \hat{w}_{MK} \\ \hat{w}_{(M-1)K} \\ \vdots \\ \overline{\hat{w}_{MK}} \end{bmatrix}. \tag{6}$$

Equations (5) and (6) show that $\boldsymbol{A}$ becomes singular as $\rho \to 0$, and tends to the identity matrix as $\rho \to K$. Therefore, the deconvolution error should decrease as $\rho$ grows toward its maximum value $K$.

Notice that the naïve choice in which $n$ spans the set $\{-M,-M+1,\cdots,+M\}$ leads to a matrix $\boldsymbol{A}'$ that becomes singular for $\rho \to 0$ as well as for $\rho \to K$. Although such behavior is undesirable, fewer harmonics are required in the computation of the associated system. Hence, in adverse noise conditions where it is only feasible to calculate the first few harmonics such a scheme might lead to better results.

### *B. THE ORTHOGONAL PROJECTION APPROACH*

Equation (4) shows that $\{\hat{w}_n\}$ is a linear combination of (shifted versions of) $\{\hat{\chi}_n\}$, with elements $\{\hat{u}_n\}$ as weights. Consequently, the problem of finding $u$ can be restated as determining the weights of this linear combination, that is, projecting the sequence $\{\hat{w}_n\}$ onto the subspace spanned by $\{\hat{\chi}_n\}$ and its shifted versions.

Taking the inner product of $\{\hat{w}_n\}$ and $\{\hat{\chi}_n^{(mK)}\}$ (see Appendix for notation) in (4), leads to

$$\sum_{n=-\infty}^{+\infty}\left(\sum_{j=-\infty}^{+\infty}\hat{\chi}_{n-jK}\hat{u}_{jK}\right)\overline{\hat{\chi}_{n-mK}} = \sum_{n=-\infty}^{+\infty}\hat{w}_n\overline{\hat{\chi}_{n-mK}} \quad . \tag{7}$$

Interchanging the summation order we get:

$$\sum_{j=-\infty}^{+\infty}\left[\left(\sum_{n=-\infty}^{+\infty}\hat{\chi}_{n-jK}\overline{\hat{\chi}_{n-mK}}\right)\hat{u}_{jK}\right] = \sum_{n=-\infty}^{+\infty}\hat{w}_n\overline{\hat{\chi}_{n-mK}} \quad . \tag{8}$$

As before, we assume that only the first $M$ harmonics are relevant. Therefore, we have

$$\sum_{j=-M}^{+M}\left[\left(\sum_{n=-\infty}^{+\infty}\hat{\chi}_{n-jK}\overline{\hat{\chi}_{n-mK}}\right)\hat{u}_{jK}\right] = \sum_{n=-\infty}^{+\infty}\hat{w}_n\overline{\hat{\chi}_{n-mK}} \quad . \tag{9}$$

As $m$ spans a set of $2M+1$ integer values suitably chosen to provide independent equations, we get a system of linear equations $\boldsymbol{Rq}=\boldsymbol{c}$ with a $(2M+1)\times(2M+1)$ matrix. Since

$\{\hat{w}_n\}$ and $\{\hat{\chi}_n\}$ exhibit complex-conjugate symmetry, the infinite summations are equivalent to elements of discrete convolutions. Hence, it further simplifies to

$$\begin{bmatrix} R_{\chi\chi}^K(0) & \overline{R_{\chi\chi}^K(1)} & \cdots & \overline{R_{\chi\chi}^K(2M)} \\ R_{\chi\chi}^K(1) & R_{\chi\chi}^K(0) & \cdots & \overline{R_{\chi\chi}^K(2M-1)} \\ \vdots & \vdots & \cdots & \vdots \\ R_{\chi\chi}^K(2M) & R_{\chi\chi}^K(2M-1) & \cdots & R_{\chi\chi}^K(0) \end{bmatrix} \begin{bmatrix} \hat{u}_{-MK} \\ \hat{u}_{(-M+1)K} \\ \vdots \\ \hat{u}_{+MK} \end{bmatrix} = \begin{bmatrix} \overline{R_{w\chi}^K(M)} \\ \overline{R_{w\chi}^K(M-1)} \\ \vdots \\ R_{w\chi}^K(M) \end{bmatrix}. \quad (10)$$

The symbol $R_{xy}^K(q)$ denotes the $qK^{\text{th}}$ element of the convolution between arbitrary sequences $x=\{\hat{x}_n\}$ and $y=\{\hat{y}_n\}$. Note that the matrix $\boldsymbol{R}$ is also a Hermitian Toeplitz matrix and it has the same behavior as the matrix $\boldsymbol{A}$, as $\rho$ spans the range from 0 to $K$.

## III. RESULTS

First, we used synthetic signals to analyze the recovered signal distortions due to the method: tests were performed for noiseless and noisy signals. Beginning with a human ECG measurement, we extracted a single QRST complex and then replicated it with a fixed frequency of 1 Hz. Then, we added to it an arbitrary periodic signal with a fundamental frequency of 5 Hz simulating an atrial signal, thereby obtaining a test signal $z$, as in Fig. 1. Also presented in this picture are a characteristic function $\chi$ used to wipe out the QRST complexes and the resulting windowed signal $w$. We used $M=4$ in all cases, thus recovering the same number of harmonics present in the simulated atrial signal.

Given $z$ and $\chi$ we obtain $w$. Then, the Fourier coefficients $\{\hat{w}_n\}$ and $\{\hat{\chi}_n\}$ are calculated by the trapezoidal integration rule in time intervals where $\chi$ is 1. We are able to build the matrix $\boldsymbol{A}$ (or $\boldsymbol{R}$, depending on the approach**)** as well as vector $\boldsymbol{c}$ (or $\boldsymbol{b}$), and to solve the related linear system. Once the vector $\boldsymbol{q}$ containing the elements $\{\hat{u}_n\}$ is known, we obtain the recovered signal

$\tilde{u}$ from its Fourier series expansion fixed by $\boldsymbol{q}$. The normalized root-mean square error is used to evaluate the difference between original and recovered signals:

$$\mathrm{NRMS} = \left( \int_0^{T_v} \left[ u(t) - \tilde{u}(t) \right]^2 dt \Big/ \int_0^{T_v} u(t)^2 dt \right)^{1/2} . \tag{11}$$

### *A. ORTHOGONAL PROJECTION APPROACH WITH NOISELESS SIGNALS*

We test the orthogonal projection algorithm with signals exhibited in Fig. 1, with the windowing ratio $\rho = 1.90$. Because the deconvolution error is quite small in this case ($\mathrm{NRMS} = 8 \cdot 10^{-4}$), the Fourier coefficients for both original and recovered signals coincide, and there is no visible difference between the two signals.

Then, we investigated the effects of the window length on the recovered signal quality. Decreasing $\rho$ to 1.00 produces neither perceivable changes in the recovered field nor in the Fourier coefficients, and there is a slight error increase: $\mathrm{NRMS} = 1 \cdot 10^{-3}$. By further reducing the windowing ratio to $\rho = 0.67$, the error grows to $\mathrm{NRMS} = 0.3$, indicating a severe decline in the recovery quality. The original and recovered signals and their Fourier coefficients are shown in Fig. 2.

Finally, for $\rho = 0.40$ there is a larger error (NRMS = 0.5), hence, a worse recovery quality, as presented in Figs. 3a and 3c. Fig. 3b shows the recovered signal superimposed with the windowed signal *w*. As expected, the recovered signal agrees with the original signal within intervals where the latter is preserved by the windowing, that is, $\left| \tilde{u}(t) - u(t) \right|$ is negligible for all *t* such that $w(t) = u(t)$ holds.

### *B. DECOMPOSITION APPROACH WITH NOISELESS SIGNALS*

We tested the decomposition approach using the same basic signals as before (see Fig. 1). The deconvolution error is $10^{12}$ smaller than the projection approach error ($\mathrm{NRMS} = 6 \cdot 10^{-16}$), indicating an outstanding recovery quality.

Then, we decrease $\rho$ until a noticeable mismatch is observed in the Fourier coefficients plot. Fig. 4 shows the results for the windowing ratio $\rho = 0.19$. Notice that such a narrow window still furnishes an acceptable recovered signal ($\mathrm{NRMS} = 8 \cdot 10^{-2}$).

A further decrease in the windowing ratio ($\rho = 0.12$) intensifies the distortions, as presented in Fig. 5 ($\mathrm{NRMS} = 0.6$). Superimposed plots of the windowed and recovered signals are also shown in this figure. As in the orthogonal projection approach both signals agree in the region where the window is 1.

### *C. ORTHOGONAL PROJECTION APPROACH WITH NOISY SIGNALS*

We investigate the additive noise influence on the recovered signal quality. To do so, we added a Gaussian white noise component $\eta$ to the test signal *z* previously described. Different levels of noise were superimposed, according to a prescribed signal-to-noise ratio (SNR). To provide a more consistent figure, the SNR (usually expressed in decibels) is calculated based on *u*, instead of *z*:

$$\mathrm{SNR} = 10\log_{10}\left[\left(\frac{1}{T_u}\int_0^{T_u} u(t)^2\,dt\right)\Big/\sigma_{noise}^2\right] = 10\log_{10}\left[\left(\sum_{n=-\infty}^{+\infty}|u_n|^2\right)\Big/\sigma_{noise}^2\right], \qquad (12)$$

where $\sigma_{noise}^2$ is the variance of $\eta$.

When noise was added, 500 recoveries were performed for distinct realizations $\eta$ with the same SNR, to obtain statistically meaningful NRMS values. Thus, the NRMS figure is displayed as *mean* ± *standard deviation*.

The results for a noisy signal with SNR = 10 dB and $\rho$ = 1.90 using the orthogonal projection approach show slight perturbations in the coefficient values, but the recovery quality is still quite good ($\mathrm{NRMS} = 2.4 \cdot 10^{-2} \pm 5.7 \cdot 10^{-3}$). By decreasing the SNR to 3 dB, which is an extremely large $\eta$ with half the power of *u*, we obtained the results shown in Fig. 6, for $\rho = 1.90$ as before. As expected, the perturbations in the coefficients grew. However, the method is quite insensitive to noise, since the error has just increased to $\mathrm{NRMS} = 5.4 \cdot 10^{-2} \pm 1.2 \cdot 10^{-2}$, as can be seen in Fig. 6b.

### *D. DECOMPOSITION APPROACH WITH NOISY SIGNALS*

Finally, we test the decomposition approach with the same SNRs used in the previous section. For SNR = 10 dB and $\rho = 1.90$ the results exhibit only slight coefficient value deviations, providing a good recovery quality ($\mathrm{NRMS} = 2.4 \cdot 10^{-2} \pm 5.8 \cdot 10^{-3}$).

For $\rho$ = 1.90 as before, the decrease of the SNR to 3 dB yielded larger coefficient deviations. Still, error increased only to $\mathrm{NRMS} = 5.3 \cdot 10^{-2} \pm 1.3 \cdot 10^{-2}$, as shown in Fig. 7.

### *E. DECOMPOSITION APPROACH WITH REAL RECORDINGS*

We used the decomposition approach to test the technique on real ECG and MCG recordings of atrial flutter episodes in humans. We reproduce in Fig. 8 the results presented in [14]. Fig. 8a shows the ECG recording *z*(*t*), the windowed signal *w*(*t*) and the recovered atrial signal $\tilde{u}(t)$ of an atrial flutter episode in an adult woman, and Fig. 8b presents the corresponding MCG signals. We notice that baseline drifts and low-frequency periodic noise are also removed

by the technique, yielding a good recovery. Even though the ventricular activity is not perfectly periodic, a periodic time window can be defined to wipe it out.

Next, we applied the technique on two recordings of atrial flutter episodes from Physiobank ECG databases [15]. The first one, shown in Fig. 9a, was selected from the MIT-BIH Atrial Fibrillation Database, whereas the second one, presented in Fig. 9b, was obtained from the MIT-BIH Arrhythmia Database.

Because both signals were digitized from old analog tape recordings, frequency changes due to tape speed variations affect the periodicity of the atrial component, mainly in the second recording. A nice property of our method is that it is still possible to recover the atrial component, despite this difficulty. Of course, the more aperiodic the digitized signal, the less the recovered signal is able to track fast variations, as seen in Fig. 9b.

## IV. DISCUSSION

The plot NRMS $\times$ $\rho$ shown in Fig. 10 summarizes the performance of the two approaches, in the absence of noise, for synthetic signals. Even though the overall behavior is similar — albeit not equal — for both methods, the decomposition approach is much better than the orthogonal projection approach as $\rho$ grows.

Nevertheless, the superiority of one approach over the other is not so clear when the recordings are corrupted by a white noise additive component. Fig. 11 shows the plot NRMS $\times$ SNR for several values of $\rho$. For a fixed $\rho$, the curves for both approaches intersect, indicating that the SNR-$\rho$ plane can be divided in regions where each of the two methods is better than the other one.

Based on the intersection of several NRMS $\times$ SNR curves we constructed the graph in Fig. 12, which shows approximately the region where each approach is optimal. The orthogonal

projection approach should be used in hard problems, i.e., whenever the signal quality is poor (low SNRs) or the windowing ratio $\rho$ is small. Otherwise, the decomposition approach should be chosen.

The transition between the two regions is not sharp, especially for large windowing ratio values, as seen in Fig. 11. For instance, the two NRMS $\times$ SNR curves for $\rho = 1.90$ are nearly coincident if the SNR is lower than 30 dB. Consequently, there exists a sizeable transition zone between the two optimal regions, which widens as $\rho$ increases. Because the results shown in Figs. 6 and 7 were obtained with parameter values lying in this transition zone, the recovery quality (and, hence, the NRMS error) is almost the same, indicating that both approaches are equivalent in such situation.

The tests performed with real ECG and MCG recordings showed that the technique yields good recovery, even in the presence of noise and of baseline drift. By increasing the number of harmonics used in each case, little change was observed in the recovered atrial signal above a certain limit (typically, from five to nine harmonics). Consequently, determining the best number of harmonics to be used in the recovered signal is a simple issue.

## V. CONCLUSION

A deconvolution-based technique is proposed to retrieve the ECG or MCG signal component related to the atrial cardiac activity. Two approaches for implementing the deconvolution problem were considered, and it was shown that each one is better suited to different ranges of signal-to-noise ratio and windowing factor values. Both approaches were successfully tested with noiseless and noisy synthetic recordings, and the decomposition approach was also tested with real recordings of atrial flutter episodes.

The technique is implemented under the assumption that the atrial activity is perfectly periodic and that the ventricular one, though not necessarily periodic, can be wiped out by a multiplicative periodic window. Any irregularity manifested in the atrial component is considered to be due to an additive noise component. Thus, our technique can be used to process recordings of several periodic tachyarrhythmias exhibiting an aperiodic ventricular activity together with a regular atrial activity, provided that the periodic time window is narrow enough to wipe out all such irregular ventricular component while leaving intact segments of the atrial component containing information for the deconvolution procedure.

An extension of the technique to handle ventricular activity with large deviations from a periodic regime, and consequently a broader class of periodic atrial tachyarrhythmias, needs to be developed. Nevertheless, the simplicity of the method will possibly be sacrificed, as more complicated signal processing will be required.

## APPENDIX

In this section we collect some facts concerning notation and conventions adopted in this paper.

*Sequences:*

We use the concise notation $\{\hat{x}_n\}$ to denote a two-sided complex-valued sequence $\{\hat{x}_n\}_{n=-\infty}^{+\infty}$. The symbol $\{\hat{x}_n^{(M)}\}$ stands for the sequence $\{\hat{x}_n\}$ shifted *M* elements to the right. That is,

$$\text{for all } n \in \mathbb{Z}: \qquad \hat{x}_n^{(M)} = \hat{x}_{n-M} \ ,$$

where $M \in \mathbb{Z}$. In all cases considered, the sequences are formed by coefficients of Fourier series expansions of bounded piecewise continuous functions and, therefore, they belong to Hilbert space $\ell^2$, which is comprised of all square-summable two-sided sequences of complex-valued scalars. Hence, the framework of Hilbert spaces, such as inner products, orthogonal projections and the Fourier series Theorem, can be applied to these sequences.

*Inner products:*

We use the standard inner product for a pair of sequences in Hilbert space $\ell^2$. That is, if $x = \{\hat{x}_n\}$ and $y = \{\hat{y}_n\}$ belong to $\ell^2$ then the inner product $\langle x, y \rangle$ is given by

$$\langle x, y \rangle = \sum_{n=-\infty}^{+\infty} x_n \overline{y_n},$$

where the over-bar denotes complex conjugation.

*Fourier series:*

We use the following definition for the representation in Fourier series of a bounded and piecewise continuous function *f* of period *T*:

$$\sum_{n=-\infty}^{+\infty} \hat{f}_n e^{i2\pi nt/T} \quad ,$$

where the Fourier coefficients are given by

$$\hat{f}_n = (1/T) \int_0^T f(t) e^{-i2\pi nt/T} dt \quad , \quad \forall n \in \mathbb{Z}$$

and *i* is the imaginary unit.

By means of a theorem on convergence of Fourier series [13] we guarantee that the Fourier representation converges to $f(t)$ at each point $t \in \mathbb{R}$ where $f$ is continuous, and to the average of the left- and right-hand limits at points $t \in \mathbb{R}$ where $f$ is discontinuous.

In particular, it can be easily verified that the convolution property hold true: if $f$ and $g$ are functions satisfying the conditions previously stated and $h = f g$, then

$$\hat{h}_n = \sum_{j=-\infty}^{+\infty} \hat{f}_j \hat{g}_{n-j} = \sum_{j=-\infty}^{+\infty} \hat{g}_j \hat{f}_{n-j} \ , \ \forall n \in \mathbb{Z} \, ,$$

where $\{\hat{f}_n\}$, $\{\hat{g}_n\}$ and $\{\hat{h}_n\}$ are the Fourier coefficients of $f$, $g$ and $h$, respectively.

## REFERENCES


[1] M. Roelke and J. N. Ruskin, "Dilated cardiomyopathy: ventricular arrhythmias and sudden death," in *Cardiac Electrophysiology: From Cell to Bedside*, D. P. Zipes, J. Jalife and R. Zorab, Eds. 2nd ed, Philadelphia: Saunders, 1995, pp. 744-753.

[2] J. E. Poole and G. H. Bardy, "Sudden cardiac death," in *Cardiac Electrophysiology: From Cell to Bedside*, D. P. Zipes, J. Jalife and R. Zorab, Eds. 2nd ed, Philadelphia: Saunders, 1995, pp. 812-832.

[3] E. C. Monteiro, C. H. Barbosa, E. A. Lima, et al., "Application of a single-channel SQUID magnetometer for non-invasive study of cardiac tachyarrhythmias mechanisms," *Physica C*, vol. 354, pp. 83-86, 2001.

[4] H. Koch, "SQUID magnetocardiography: status and perspectives," *IEEE Trans. Appl. Supercond.*, vol. 11, pp. 49-59, March 2001.

[5] P. Seidel et al., "High-Tc SQUID systems for practical use," *IEEE Trans. Appl. Supercond.*, vol. 9, pp. 4077-4080, June 1999.

[6] E. C. Monteiro, S. DellaPenna, L. DiDonato, et al., "The study of steady magnetic fields associated with primary and secondary ST shift in ischaemic rabbit hearts," *Physiol. Meas.*, vol. 18, pp. 191-200, 1997.

[7] J. P. Wikswo Jr, "SQUID magnetometers for biomagnetism and nondestructive testing: important questions and initial answers," *IEEE Trans. Appl. Supercond.*, vol. 5, pp. 74-120, June 1995.

[8] N. V. Thakor and Y. Zhu, "Applications of adaptive filtering to ECG analysis: noise cancellation and arrhythmia detection," *IEEE Trans. Biomed. Eng.*, vol. 38, pp. 785-794, August 1991.

[9] S. Shkurovich, A. V. Sahakian and S. Swiryn, "Detection of atrial activity from high-voltage leads of implantable ventricular defibrillators using a cancellation technique," *IEEE Trans. Biomed. Eng.*, vol. 45, pp. 229-234, February 1998.

[10] M. Holm, S. Pehrson, M. Ingemansson, et al., "Non-invasive assessment of the atrial cycle length during atrial fibrillation in man: introducing, validating and illustrating a new ECG method," *Cardiovasc. Res.*, vol. 38, pp. 69-81, 1998.

[11] M. Stridh and L. Sörnmo, "Spatiotemporal QRST cancellation techniques for analysis of atrial fibrillation," *IEEE Trans. Biomed. Eng.*, vol. 48, pp. 105-111, January 2001.

[12] M. Stridh, L. Sörnmo, C. J. Meurling and S. B. Olsson, "Characterization of atrial fibrillation using the surface ECG: time-dependent spectral properties," *IEEE Trans. Biomed. Eng.*, vol. 48, pp. 19-27, January 2001.

[13] G. P. Tolstov, *Fourier Series*. Englewood Cliffs:Prentice-Hall, 1976, chapter 3.

[14] E. A. Lima, D. Marchesin, E. C. Monteiro and B. Gundelach, "Extraction of atrial cardiac activity from MCG recordings of periodic tachyarrhythmias in humans," in *Proceedings of BIOMAG 2002*, H. Nowak, J. Haueisen, F. Gieβler and R. Huonker, Eds., Berlin: VDE Verlag, 2002, pp. 1030-1032.

[15] A. L. Goldberger, L. A. N. Amaral, L. Glass, et al. (2000, June). PhysioBank, PhysioToolkit, and Physionet: components of a new research resource for complex physiologic signals. *Circulation (Circulation Electronic Pages)* [Online] *101(23*), pp. e215-e220. Available: http://circ.ahajournals.org/cgi/content/full/101/23/e215.

ACKNOWLEDGMENT

The authors would like to thank Elisabeth Costa Monteiro for helpful discussions. This work was supported in part by IMPA, CNPq under Grant 300204/83-3, and FAPERJ under Grant E-26/150.670/2001.

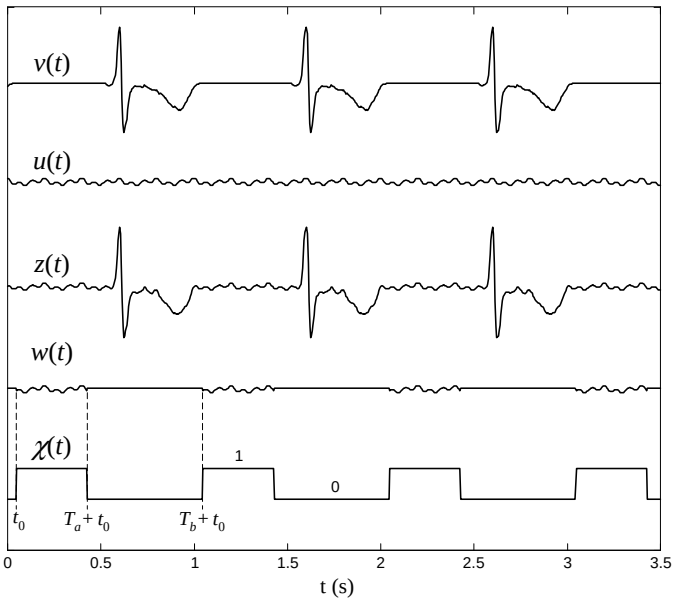


1

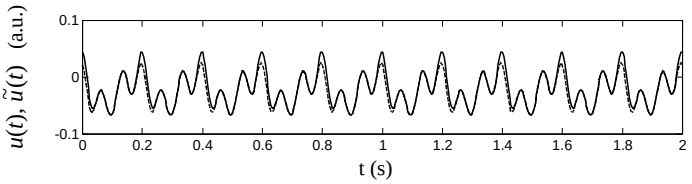
0.1
0
-0.1
0
0.2
0.4
0.6
0.8
1
1.2
1.4
1.6
1.8
2
t (s)
u(t), ũ(t) (a.u.)

(a)

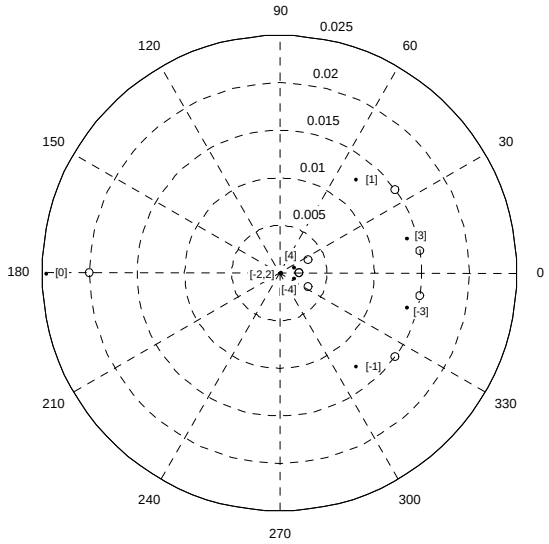
90
0.025
120
60
0.02
0.015
150
30
0.01
[1]
0.005
[3]
[4]
180
[0]
[-2,2]
[-4]
0
[-3]
[-1]
210
330
240
300
270

(b)

2

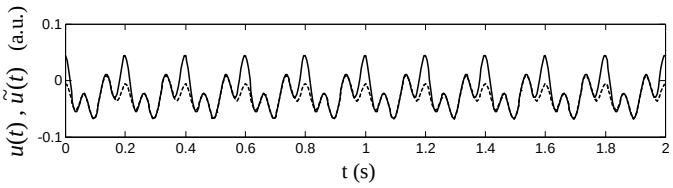
0.1
0
-0.1
0
0.2
0.4
0.6
0.8
1
1.2
1.4
1.6
1.8
2
t (s)
$u(t)$ , $\tilde{u}(t)$ (a.u.)

(a)

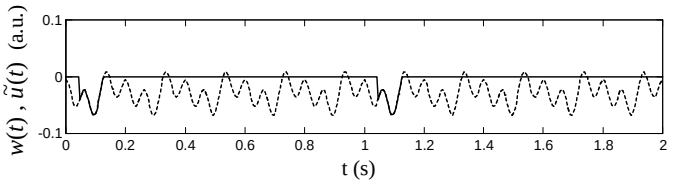
0.1
0
-0.1
0
0.2
0.4
0.6
0.8
1
1.2
1.4
1.6
1.8
2
t (s)
$w(t)$ , $\tilde{u}(t)$ (a.u.)

(b)

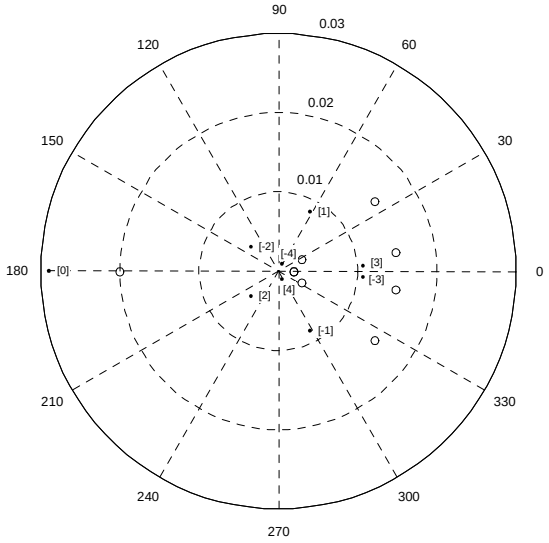
90
0.03
120
60
0.02
150
30
0.01
180
0
210
330
240
300
270
[1]
[-2]
[-4]
[3]
[-3]
[0]
[2]
[4]
[-1]

(c)

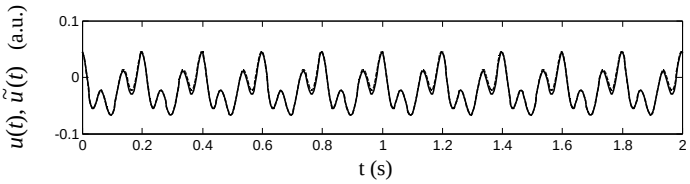
0.1
0
-0.1
0
0.2
0.4
0.6
0.8
1
1.2
1.4
1.6
1.8
2
t (s)
u(t), ũ(t) (a.u.)

(a)

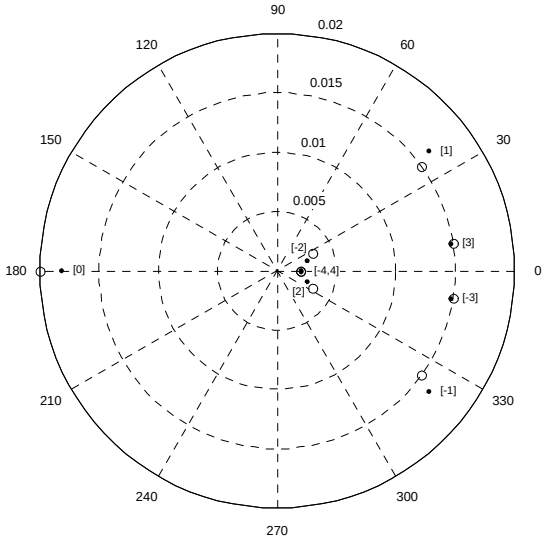
90
0.02
120
60
0.015
150
30
0.01
[1]
0.005
[3]
180
[0]
[-2]
[-4,4]
0
[2]
[-3]
[-1]
210
330
240
300
270

(b)

4

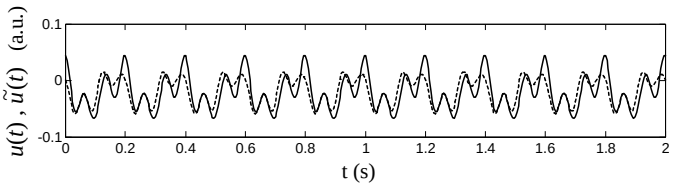
0.1
0
-0.1
0
0.2
0.4
0.6
0.8
1
1.2
1.4
1.6
1.8
2
t (s)
u(t) , ũ(t) (a.u.)

(a)

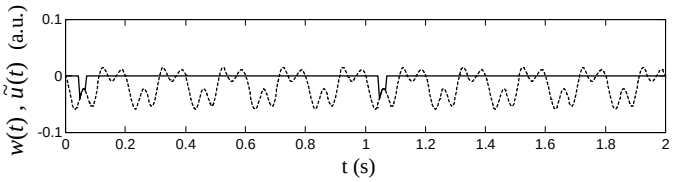
0.1
0
-0.1
0
0.2
0.4
0.6
0.8
1
1.2
1.4
1.6
1.8
2
t (s)
w(t) , ũ(t) (a.u.)

(b)

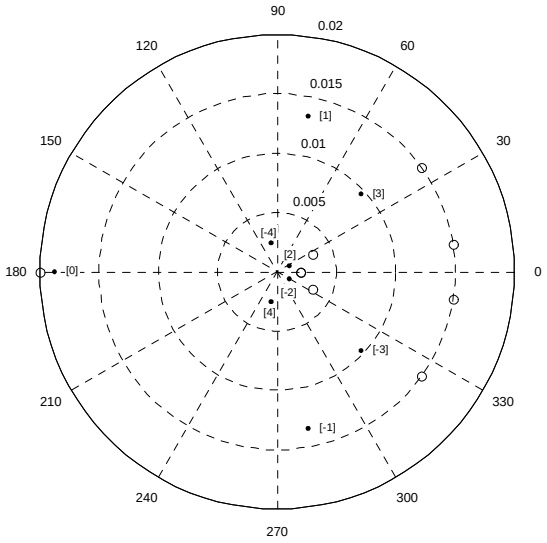
90
0.02
120
60
0.015
[1]
150
0.01
30
[3]
0.005
[-4]
[2]
180
[0]
0
[-2]
[4]
[-3]
210
330
[-1]
240
300
270

(c)

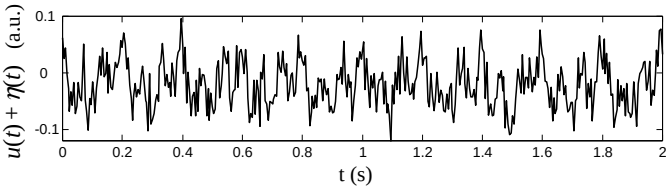
0.1
0
-0.1
$u(t) + \eta(t)$ (a.u.)
0 0.2 0.4 0.6 0.8 1 1.2 1.4 1.6 1.8 2
t (s)

(a)

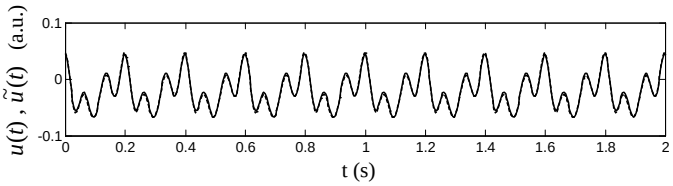
0.1
0
-0.1
$u(t)$ , $\tilde{u}(t)$ (a.u.)
0 0.2 0.4 0.6 0.8 1 1.2 1.4 1.6 1.8 2
t (s)

(b)

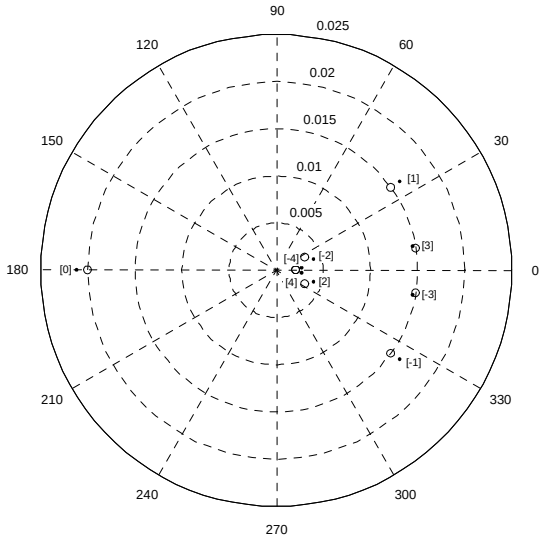
90
0.025
120
60
0.02
0.015
150
30
0.01
0.005
[1]
[3]
[-4]
[-2]
180
[0]
0
[4]
[2]
[-3]
[-1]
210
330
240
300
270

(c)

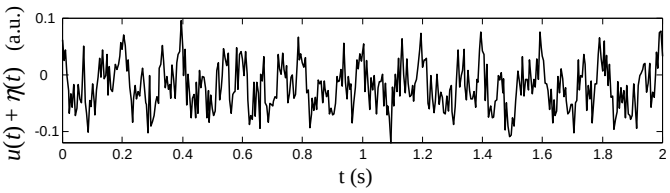
0.1
0
-0.1
$u(t) + \eta(t)$ (a.u.)
0 0.2 0.4 0.6 0.8 1 1.2 1.4 1.6 1.8 2
t (s)

(a)

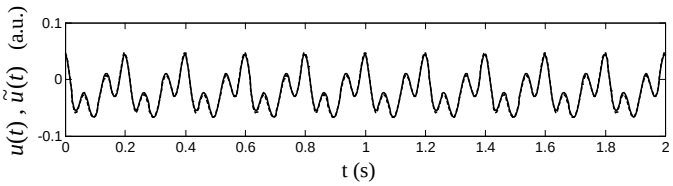
0.1
0
-0.1
$u(t)$ , $\tilde{u}(t)$ (a.u.)
0 0.2 0.4 0.6 0.8 1 1.2 1.4 1.6 1.8 2
t (s)

(b)

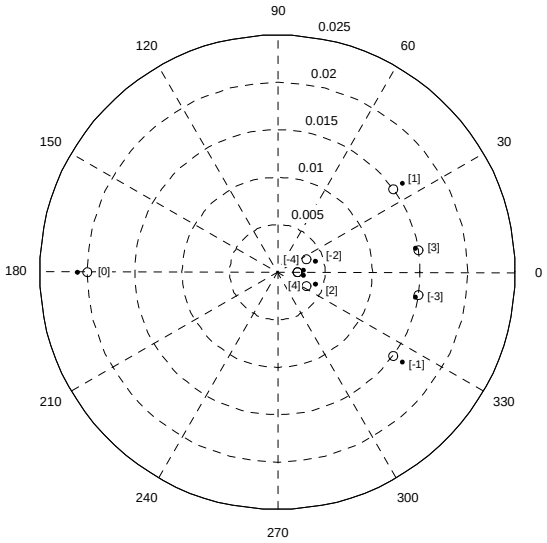
90
0.025
120
60
0.02
0.015
150
30
0.01
[1]
0.005
[3]
[-4]
[-2]
180
[0]
0
[4]
[2]
[-3]
[-1]
210
330
240
300
270

(c)

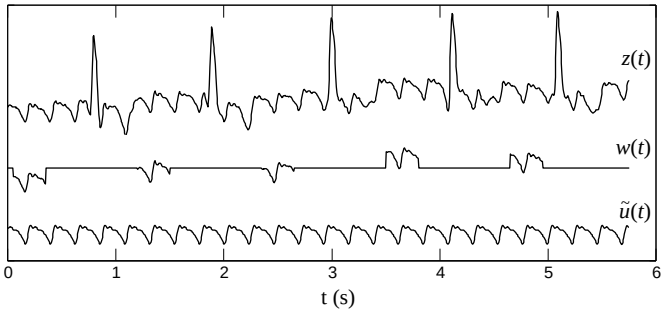


(a)

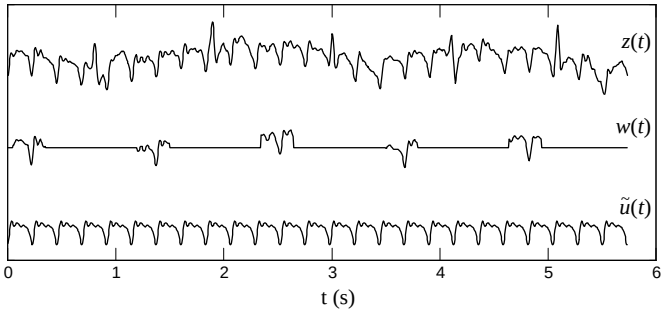


(b)

8

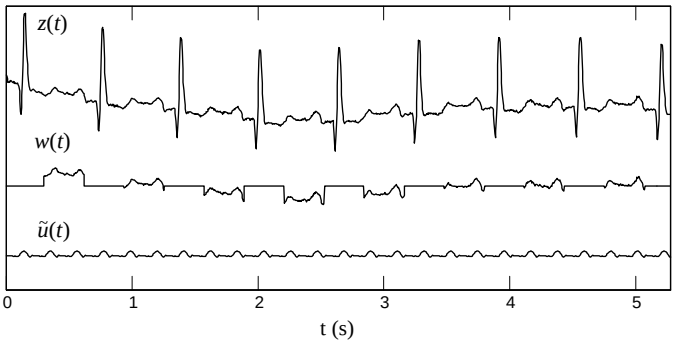


(a)

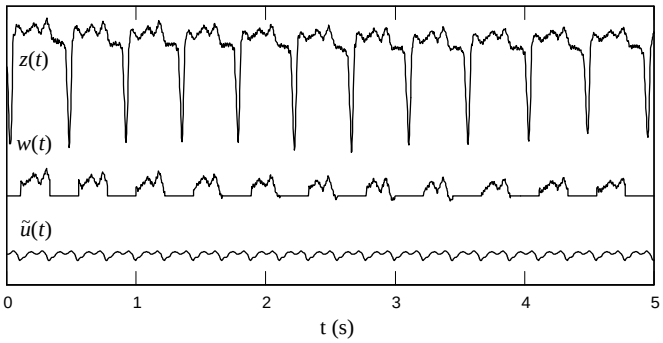


(b)

9

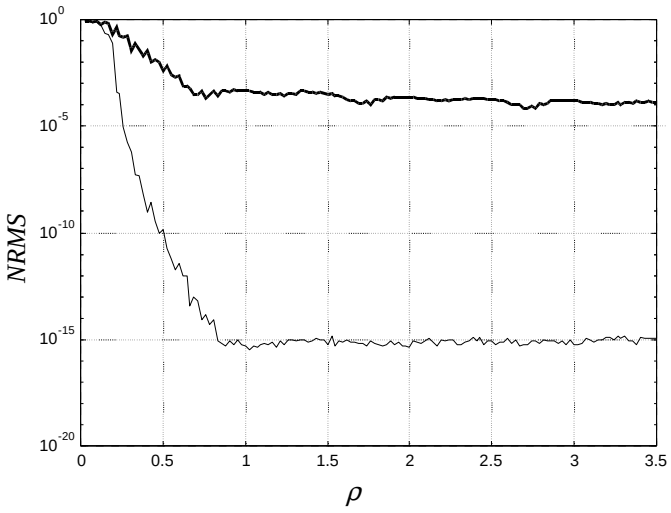


10

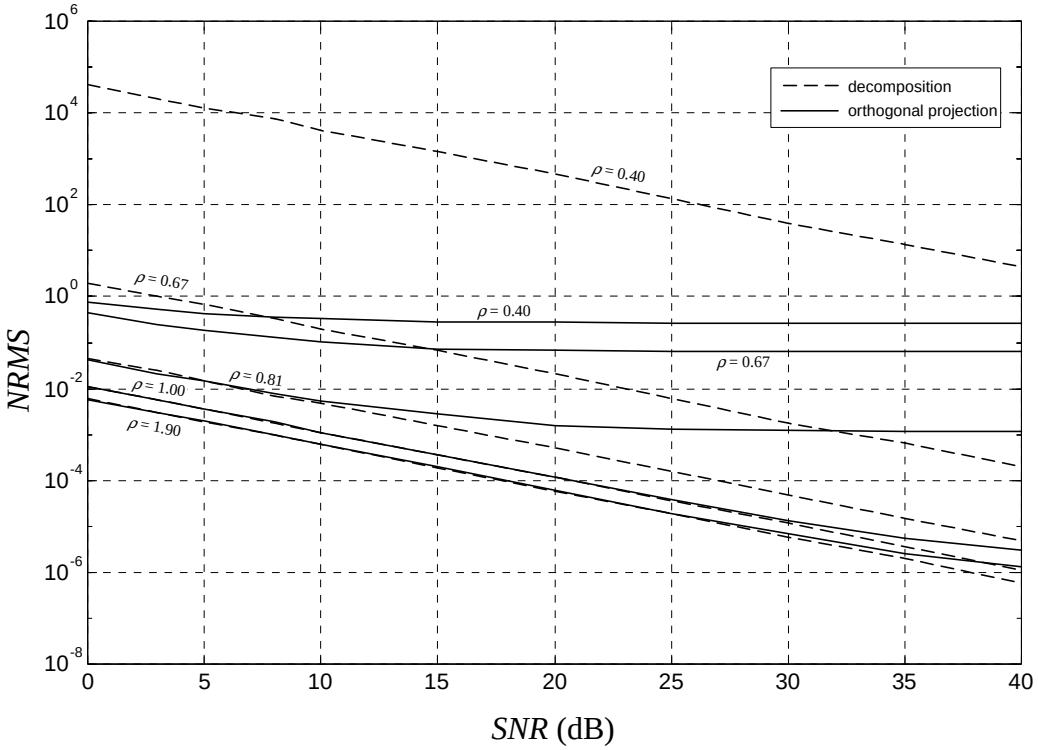
decomposition
orthogonal projection
ρ = 0.40
ρ = 0.67
ρ = 0.40
ρ = 0.67
ρ = 0.81
ρ = 1.00
ρ = 1.90
NRMS
SNR (dB)

11

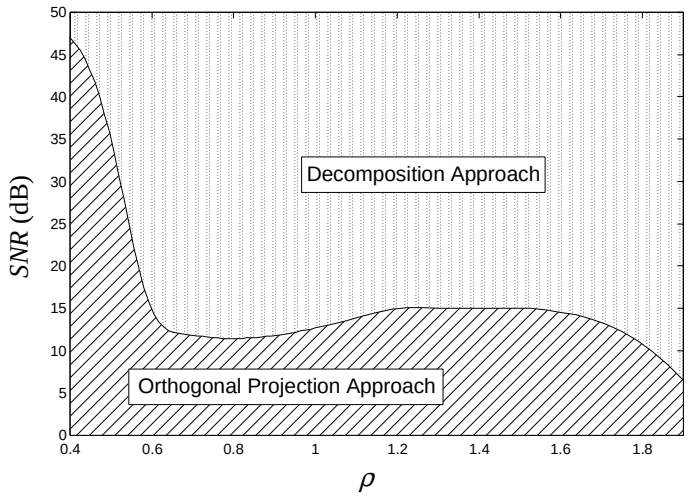
Decomposition Approach
Orthogonal Projection Approach
SNR (dB)
ρ
50
45
40
35
30
25
20
15
10
5
0
0.4
0.6
0.8
1
1.2
1.4
1.6
1.8

12

Fig. 1: Masking signal ($v$ component), simulating the ventricular activity (QRST complexes); signal of interest, simulating the atrial activity ($u$ component); resulting signal $z$, comprising the sum of both components; windowed signal $w$ for the characteristic function shown in the last plot; example of a characteristic function $\chi$ used to wipe out the QRST complexes.

Fig. 2: (a) Original signal of interest (solid line) and recovered signal for $\rho = 0.67$ using the orthogonal projection approach (dashed line). (b) Original (o) and recovered (•) Fourier coefficients.

Fig. 3: (a) Original signal of interest (solid line) and recovered signal for $\rho = 0.40$ using the orthogonal projection approach (dashed line). (b) Recovered signal (dashed line) superimposed to the windowed signal $w$ (solid line). (c) Original (o) and recovered (•) Fourier coefficients.

Fig. 4: (a) Original signal of interest (solid line) and recovered signal for $\rho = 0.19$ using the decomposition approach (dashed line). (b) Original (o) and recovered (•) Fourier coefficients.

Fig. 5: (a) Original signal of interest (solid line) and recovered signal for $\rho = 0.12$ using the decomposition approach (dashed line). (b) Recovered signal (dashed line) superimposed to the windowed signal $w$ (solid line). (c) Original (o) and recovered (•) Fourier coefficients.

Fig. 6: (a) Signal of interest contaminated by noise (SNR = 3 dB). (b) Original signal of interest (solid line) and recovered signal for $\rho = 1.90$ using the orthogonal projection approach (dashed line). (c) Original (o) and recovered (•) Fourier coefficients.

Fig. 7: (a) Signal of interest contaminated by noise (SNR = 3 dB). (b) Original signal of interest (solid line) and recovered signal for $\rho = 1.90$ using the decomposition approach (dashed line). (c) Original (o) and recovered (•) Fourier coefficients.

Fig. 8: Original recording $z(t)$, windowed signal $w(t)$ and recovered atrial component $\tilde{u}(t)$ using five harmonics, for an atrial flutter episode. (a) ECG recording. (b) MCG recording.

Fig. 9: Original ECG recording $z(t)$, windowed signal $w(t)$ and recovered atrial component $\tilde{u}(t)$ for two atrial flutter episodes. (a) First episode, with eight harmonics used in the recovered signal. (b) Second episode, with seven harmonics used in the recovered signal.

Fig. 10: NRMS $\times \rho$ plots for both decomposition (regular line) and orthogonal projection (thick line) approaches.

Fig. 11: NRMS $\times$ SNR plots for several values of the windowing factor $\rho$.

Fig. 12: Approximate best performance regions for both decomposition and orthogonal projection approaches.